Period locking due to delayed feedback in a laser with saturable absorber

T. W. Carr*

Department of Mathematics, Southern Methodist University, Dallas, Texas 75275-0156, USA

We consider laser with saturable absorber operating in the pulsating regime that is subject to delayed feedback. Alone, both the saturable absorber and delayed feedback cause the clockwise output to become unstable to periodic output via Hopf bifurcations. The delay feedback causes the laser pulse period to lock to an integer fraction of the feedback time. We derive a map from the original model to describe the periodic pulsations of the laser. Equations for the period of the laser predict the occurrence of the different locking states as well as the value of the pump when there is a switch between the locked states.

PACS number(s): 05.45.−a, 42.65.Sf, 42.60.Gd

I. INTRODUCTION

In this paper we investigate the effect of delayed feedback (DF) on a laser containing an intracavity saturable absorber (LSA). Lasers with a saturable absorber (SA) have long been used to generate high-intensity pulses. The effect of the absorber is to passively modulate the cavity losses so that the LSA is "self-pulsing." The pulsed output is of practical interest for applications that require extremely short high-peak-power pulses of light such as spectroscopy (see Refs. [1,2] for background and historical references). We introduce DF in the intensity-loss term of a rate-equation model of the class-*B* LSA as a first step to understanding the combined SA and DF effects; class-*B* lasers are those where the polarization variable can be adiabatically eliminated [3] and includes solid-state, CO_2 and semiconductor lasers. Our results will describe the locking phenomena of the LSA period to integer fractions of the delay time.

The study of the effect of delay on optical systems has produced important theoretical practical and results. For example, the effect of delay on the pulses in a passive ring cavity was studied by Ikeda [4,5]; the resulting "Ikeda Map" is ubiquitous in introductory studies of dynamical systems [6]. Arecchi *et al.* [7] studied delay in a class-*B* CO_2 laser and found complex dynamics that, for certain parameter values, were describable by Ikeda map. Of great current interest is the effect of delay on semiconductor lasers because of their widespread use in applications such as telecommunications and optical data storage devices. Lang and Kobayashi [8] formulated a rate-equation model for semiconductor lasers, subject to delay that is the starting point for many of today's theoretical studies. Common to the above systems is period locking (or frequency locking), where the period of the oscillations is related by an integer to the delay time. In lasers, this is understood to result from an interference effect between the laser-cavity modes and external-cavity modes, the latter formed by the laser facet and the exterior reflecting surface [8].

For LSAs with high-intensity pulsations, some results regarding the effect of delay have been discussed by van Tartwijk and San Miguel [9]. They numerically investigated

the effect of DF in self-pulsing semiconductor lasers; their purpose was to better quantify the statistical properties of the pulse amplitude and repetition rate due to stochastic noise. In a recent study [10] we determined the conditions for the onset of oscillations and pulsations due to the presence of a SA and delay feedback. Both the SA and DF cause the laser's clockwise (CW) output to become unstable through Hopf bifurcations. The main result of that study was that the SA can increase the sensitivity of the laser to DF. Or, the DF can cause self-pulsations outside the normal range of pump values for the LSA.

In the high-intensity pulsating regime there is a lack of theoretical results concerning the combined effects of a SA and DF. In numerical simulations the pulsations require highly accurate computations that take long times. From an analytical perspective, the pulsating output is highly nonlinear and typical perturbation approximation techniques fail. Grigorieva et al. [11–13] and Pieroux and Erneux [14] have developed asymptotic methods to analyze pulsating laser output with delay, which are based on ideas from boundary-layer theory. In this paper we use this general technique to obtain our first results concerning the effect of DF on the LSA's pulsating output. In particular, we investigate the effect of DF on the period and intensity of the pulses produced by the LSA.

We consider a nondimensionalized model for the class-*B* LSA with the addition of a delay term [2,15,16]:

$$\frac{dI}{dt} = \left(D + \frac{A_2}{1 + aI} - 1 \right) I + \eta I(t - \tau),$$

$$\frac{dD}{dt} = \gamma [A_1 - (1 + I)D], \qquad (1)$$

where I is the intensity and D is the population inversion. Parameter γ is the inversion-decay rate normalized by the cavity-decay rate and is typically small; the strongly pulsating behavior of the LSA is directly related to the small values of γ [17]. A_1 is the pump or injected current in the case of semiconductor lasers. $A_2 < 0$ is defined as the absorber-pump parameter and a describes the relative saturability of the absorber with respect to the active media. The feedback

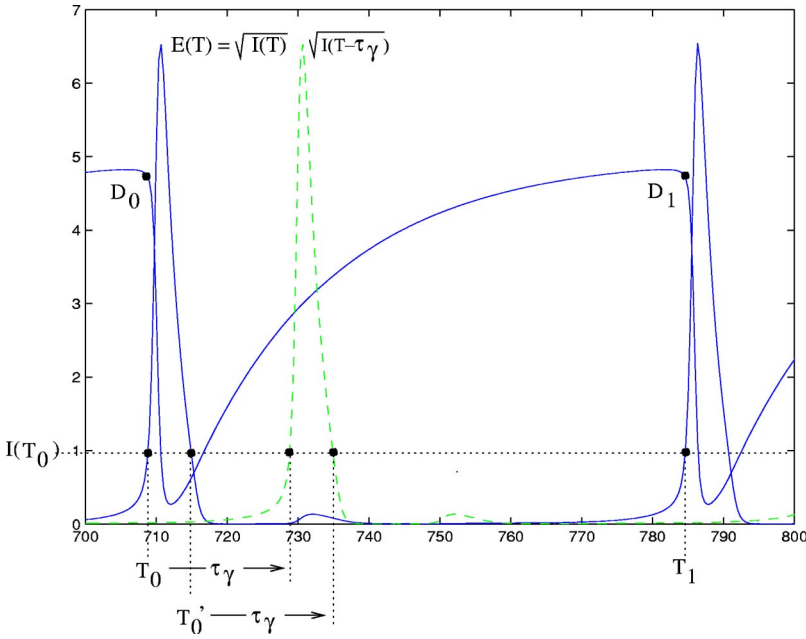*Email address: tcarr@mail.smu.edu

FIG. 1. Bifurcation diagram [23] of the LSA without feedback ($\eta=0$). Solid (dotted) lines are stable (unstable) solutions. $A_{1th}=4.5$ is the bifurcation of the zero steady state to the nonzero steady state. $A_{1lp}=4.1$. $A_{1h}=7.8$ is the Hopf bifurcation to periodic solutions that are unstable. Pulsating solutions occur on the upper branch between $A_{1hlp}=9.6$ and A_{1th}, where they terminate in a homoclinic orbit ($A_2=-3.5$, $a=2$, $\gamma=0.05$).

strength is given by η and delay by τ. Equations (1) are commonly referred to as delay differential equations (DDE) due to the DF term.

In Eqs. (1) the DF corresponds to a delayed loss in the real-valued intensity. A delayed-loss term is possible to implement with an electro-optic feedback loop [7]. However, a delayed version of the real intensity may be more difficult to realize experimentally. A field reinjected due to reflection from an external surface, is properly modeled by considering the complex-valued electric field. This requires evolution equations for both the field's amplitude and phase and greatly complicates the analysis. As a first step in this investigation we consider the simpler equations (1).

Self-pulsation of the LSA without feedback ($\eta=0$) appears through a bifurcation mechanism that we briefly review for the case shown in Fig. 1. The laser-first threshold occurs when $A_1=A_{1th}\equiv 1-A_2$, and the nonzero steady state (NZSS) may appear through either a supercritical or subcritical bifurcation. In Fig. 1 we show the bifurcation diagram for the subcritical case. A Hopf bifurcation to pulsating solutions appear on the nonzero branch of solutions at A_{1h} and is subcritical so that the oscillatory solutions are unstable. The oscillations become stable pulsations as the branch passes the turning point at A_{1hlp}. As A_1 is decreased, the oscillations become increasingly pulsating with increasing interpulse periods. The branch terminates at a homoclinic orbit of infinite period as A_1 approaches A_{1th}. We note that the unstable branch of oscillatory solutions serves as a basin boundary between the NZSS and the pulsating solutions for $A_{1h}<A_1<A_{1hlp}$.

In the following section, we describe period locking for long delays using results from numerical simulations. Then, in Sec. III we present a map that describes the dynamics of the pulsating output. The map is derived from the DDE model (1) and the details of the derivation are shown in Appendix A. We derive simplified results for periodic pulsations in Sec. III B and then analyze these in detail while comparing to numerical simulations in Sec. IV. We finish with a discussion in Sec. V.

II. PERIOD LOCKING

In the LSA without DF ($\eta=0$), as the pump is increased from threshold A_{1th}, the period decreases smoothly to a finite value near the upper Hopf-bifurcation point. This is shown by the thick decreasing curve in Fig. 3(a). This curve serves as a reference for the thick stepped curves which are the result of numerical simulations of the LSA with DF ($\eta\neq 0$) when $\tau=50$. The steps in the period correspond to period locking that we will describe in detail below. We used the MATLAB routine DDE23 [18] to numerically integrate Eqs. (1) rewritten in terms of the electric field, where $I=|E|^2$. The latter is done to avoid accuracy problems resulting from the high-amplitude pulsations. All parameters values are the same as Fig. 2 unless otherwise noted.

As stated above, the thick-solid stepped curve in Fig. 3(a) is the period of the LSA with DF ($\eta\neq 0$). When the pump is near threshold the laser locks to a period determined by the delay, $P\approx\tau$. As the pump is increased the period approaches that of the LSA's natural period. Before exceeding the natural period, the laser's period jumps down and locks to $P\approx\tau/2$. We will show later that, in general, the period locks to an integer fraction of the delay, $P\approx m+1$, m an integer.

If the pump is such that the laser is initially locked to $P\approx\tau/2$ then as the pump is decreased we find a region of hysteresis. That is, the period stays locked to $P\approx\tau/2$ for values of the pump lower than when the period step down from $P\approx\tau$. As the pump is decreased further, there is a critical value when the period steps up and locks to $P\approx\tau$. As an additional demonstration of period locking, Fig. 4 shows the case of $\tau=100$. Because the delay is longer, the period-locking phenomena is even more dramatic. In this case the lock states correspond to $P\approx 100$, 50, 33, and 25. The LSA's natural period is an upper bound on the period of the LSA
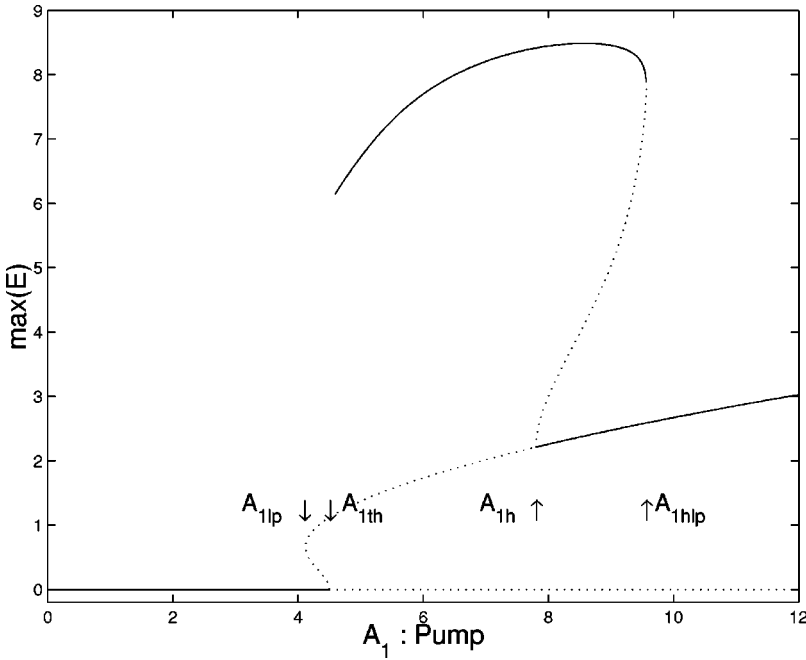
FIG. 2. For two subsequent pulses the map variables T_n and D_n are shown. The electric field, equal to the square root of the intensity, is plotted so that its magnitude is comparable to the inversion and they can be seen on the same graph. The time-delayed pulse is shown as a dashed line ($\eta = 0.04, \tau = 20, A_1 = 8, A_2 = -3.5, \quad a = 2, \quad \gamma = 0.05$).

with DF. Hence, as the pump is increased the period steps down from one locked state to another as the natural period curve is approach. There is again a hysteresis effect as the pump is decreased. The period stays locked to a lower step for pump values smaller than where the step down occurred. In fact, the pump regions for locking to a particular period do not even overlap.

III. PULSING DDES TO A MAP

A. Derivation of the map

The pulsing behavior of the laser is analyzed by using approximation techniques based on matched asymptotic expansions [19] to derive a map. We previously used this method to analyze pulsations in driven class-*B* lasers [20] and LSAs [15]. We also benefited from the work of Grigorieva *et al.* [11–13] as a guide to handling the DF. We will only summarize the method and present the details in Appendix A.

During the interval of time from one pulse to the next, there are subintervals where different terms in Eqs. (1) are large or small. From Fig. 2 we see that the intensity is large during the initial short subinterval reminiscent of a boundary layer or inner solution. After the pulse there is a longer subinterval where the intensity is very small corresponding to the outer solution. However, during this time there is a short subinterval where the delayed-pulse term becomes large. In each of these subintervals, we solve approximate equations for the laser with the appropriate assumptions regarding large and small terms. The initial conditions for each subinterval are determined by the terminal conditions from the previous subinterval. By patching the results from one subinterval to the next, we determine the state of the system at T_1, based on the state of the system at T_0. In general, this results in a map from T_n to T_{n+1}.

Depending on the operating conditions of the laser, it is often the case that the delay is longer than the time between pulses. In this case, the large delayed pulse that occurs in the current interval of time is not due to the pulse at the start of that interval. Instead, it is due to the delayed pulse from an earlier interval of time. This introduces a retarded or delayed index in the map because interval n depends on a pulse from interval $n-m$.

The map we obtain is

$$D_{n+1} = A_1 + (G_n - A_1)e^{-P_n}, \tag{2}$$

$$T_{n+1} = T_n + P_n, \tag{3}$$

where T_n is the time when population inversion D_n is a maximum. [Time has been rescaled according to $T = \gamma t$ so that the interval between pulses is $O(1)$.] The time and inversion at $n+1$ are determined by their previous values and the period of time between pulse P_n and inversion minimum G_n. These latter quantities are determined by a set of implicit equations given by

$$0 = \ln\left(\frac{G_n}{D_n}\right) - (G_n - D_n),$$

$$\frac{\eta}{\gamma}p_{n-m} = e^{C_1} - e^{C_2},$$

$$D_n - p_n = D_n e^{-p_n},$$

$$C_1\gamma = -\lambda(P_n - \xi_n) + (G_n - A_1)(e^{-P_n} - e^{-\xi_n}),$$

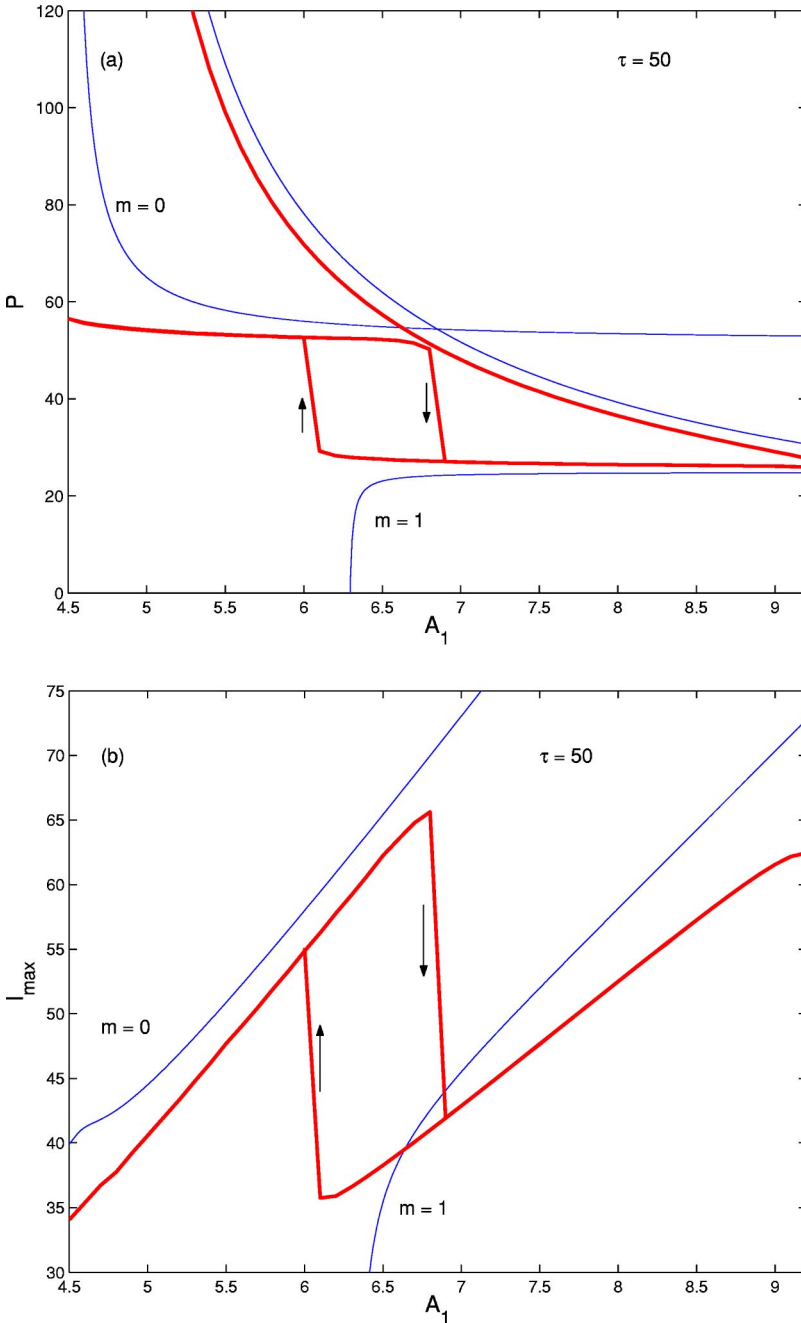$$C_2\gamma = \lambda\xi_n + (G_n - A_1)(1 - e^{-\xi_n}),$$

FIG. 3. In both (a) and (b), thin curves correspond to analytical results while the thick curves are from numerical simulations. (a) Period vs. pump. The right-most decaying curves are for the case of no DF, $\eta = 0$. The map predicts that the period becomes large as $\lambda \rightarrow 0$ and the homoclinic orbit is approached. In the presence of DF ($\eta \neq 0$) there is exponential decay of the period until it locks. When the period equals the natural period, $\eta = 0$, it switches from the $m = 0$ curve to the $m = 1$ curve. (b) Intensity vs. pump. As the pump is increased, the intensity of the pulses increases. At the switch point, the intensity abruptly decreases and then follows the new branch of solutions for increasing pump. Parameter values are the same as Fig. 2 except for τ and A_1.

$$\xi_n = \begin{cases} \tau_\gamma - \displaystyle\sum_{j=1}^{m} P_{n-j}, & m \geq 1 \\ \tau_\gamma, & m = 0, \end{cases} \quad (4)$$

where $\lambda = A_1 - A_{1th}$ [see Eq. (A10)] is how far the laser is pumped beyond threshold. The delay time is accounted for by variable ξ_n which is the subinterval of time from the most recent pulse to the delayed pulse in that interval. The strength of the delayed pulse is accounted for by p_{n-m} which is related to the energy of the pulse at time T_{n-m} [see Eq. (A6)]. Finally, we note that if the DF is removed by setting $\eta = 0$ and $\tau_\gamma = \tau\gamma = 0$ then the simplified map is identical to the one we derived in Ref. [15].

B. Periodic pulsations

One motivation for deriving a map is that iterating the map is typically much easier and quicker than numerically simulating the original flow from which it was derived. In the present case, however, the map consists of nonlinear, coupled implicit equations that are very difficult to solve. Transients or chaotic behavior are better simulated using the original differential equation. However, the map is very useful for studying periodic solutions that correspond to fixed points of the map. The resulting equations are still difficult to solve, but with further approximations we will obtain excellent results.

As stated above, fixed points of the map correspond to periodic solutions of the original system. Thus, all variables
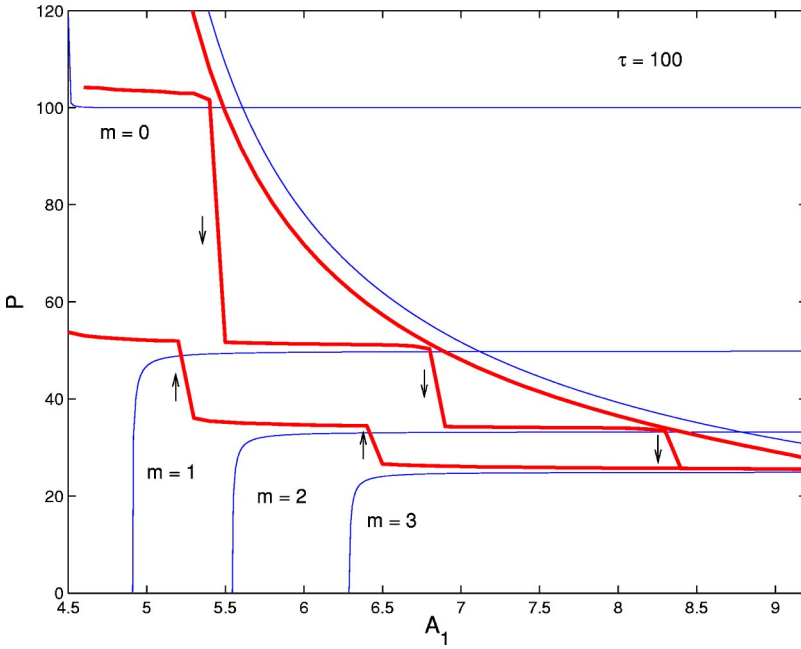
FIG. 4. Large delay allows for more locking regions, $P \approx \tau_\gamma/(m+1)$. Analytical predictions for the switch points are indicated. Thin curves, analytical; thick curves, numerical.

(except for time) are constants independent of index n.

$$D = A_1 + (G - A_1)e^{-P},$$

$$T_{n+1} = T_n + P, \tag{5}$$

$$0 = \ln\left(\frac{G}{D}\right) - (G - D), \tag{6}$$

$$\frac{\eta}{\gamma}p = e^{C_1} - e^{C_2}, \tag{7}$$

$$D - p = De^{-p}, \tag{8}$$

$$C_1\gamma = -\lambda(P - \xi) + (G - A_1)(e^{-P} - e^{-\xi}),$$

$$C_2\gamma = \lambda\xi + (G - A_1)(1 - e^{-\xi}),$$

$$\xi = \tau_\gamma - mP, \quad m = 0,1,2,\ldots.$$

Our first qualitative result for the period is determine by Eq. (7), which can be written as

$$\frac{\eta}{\gamma}p = e^{C_1}\left(1 - \exp\left\{\frac{1}{\gamma}[\lambda P + (G - A_1)(1 - e^{-P})]\right\}\right).$$

The right-hand side must be positive because p is related to the energy of the pulse. Thus, the exponent on the right-hand side must be negative:

$$\lambda P + (G - A_1)(1 - e^{-P}) < 0. \tag{9}$$

This equation, when made an equality, is exactly the equation for the LSA's natural period without DF [15]. That is, if P_0 is the LSA's natural period, $\lambda P_0 + (G - A_1)[1 - \exp(-P_0)] = 0$. By combining these last two equations we obtain

$$\lambda P + (G - A_1)(1 - e^{-P}) < \lambda P_0 + (G - A_1)(1 - e^{-P_0}).$$

Some algebra and the assumption that $G \approx 0$ (see next paragraph) leads to the conclusion that $P < P_0$; the period with feedback must be less than the LSA's natural period without feedback. In Appendix A we show that this is identical to the condition for asymptotic validity of the map-construction technique.

We now use the result that P is less than the natural period and make two approximations that greatly simplify the conditions for periodicity. The first is that for pulsating solutions, where the minimum of the inversion is very close to zero, $G \approx 0$. Second, the energy in the pulse is large so that $\exp(-p) \ll 1$. We discuss the details and validity of the approximations further in Appendix B. Their application leads to a single implicit equation for the period that then determines the inversion:

$$\lambda(P - \xi) + A_1(e^{-P} - e^{-\xi}) = -\gamma \ln\left[\frac{\eta}{\gamma}A_1(1 - e^{-P})\right], \tag{10}$$

$$D = A_1(1 - e^{-P}). \tag{11}$$

A numerical solution for period P is now much easier to obtain than if we had used the original fixed-point equations. However, we can obtain explicit results for P with two additional approximations.

Suppose that $P - \xi = (m+1)P - \tau_\gamma \ll 1$. We refer to this as the locking approximation because the laser period is an integer multiple of the delay. To find P we let $P = (\tau_\gamma + P_1)/(m+1)$ and solve for $P_1 \ll 1$. The final result for P is

$$\text{LA:} \quad P = \frac{\tau_\gamma}{m+1} - \frac{\gamma}{m+1}\frac{\ln\left[\frac{\eta}{\gamma}A_1(1 - e^{-\tau_\gamma/(m+1)})\right]}{[A_1(1 - e^{-\tau_\gamma/(m+1)}) - A_{1th}]}, \tag{12}$$
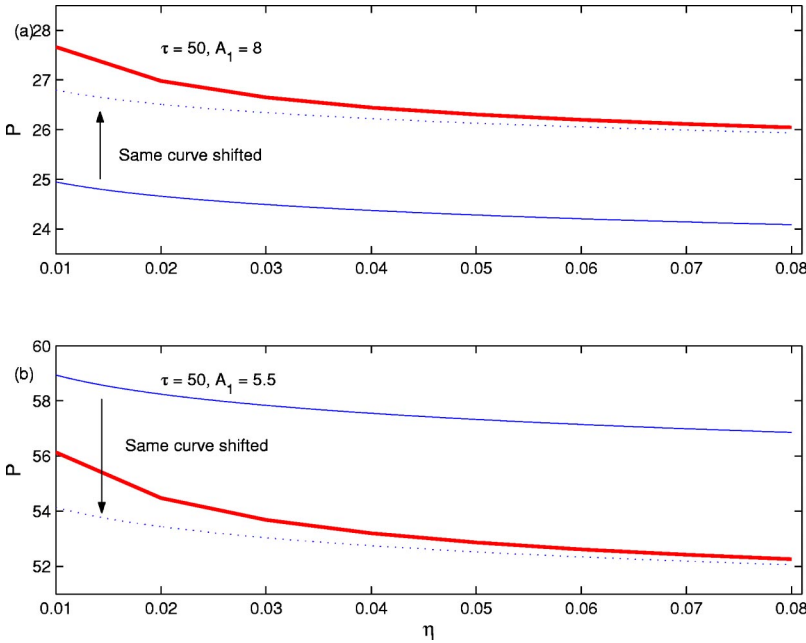
FIG. 5. Period as a function of the feedback strength η for two different values of the pump. Thin curves, analytical; thick curves, numerical. The dotted curve is a shifted version of the analytical result for better visual comparison.

where we have dropped an $O(\gamma)$ term in the denominator of the correction. We will refer to the locking-approximation result for P in Eq. (12) as LA.

If the lasers are not locked, the period is typically large enough so that $e^{-P} \ll 1$. Also, in general, we need only consider case $m = 0$ because when $m \geq 1$ the solutions are locked and better described by LA. Now we find that

$$\text{UA:} \quad P = \tau_\gamma + \frac{A_1}{\lambda} e^{-\tau_\gamma} - \frac{\gamma}{\lambda} \ln\left[\frac{\eta}{\gamma} A_1\right]. \quad (13)$$

We will refer to this "unlocked" approximation for the period, Eq. (13), as UA. The LA and UA results are equivalent in limit $\tau_\gamma \to \infty$ ($m = 0$).

We note that in Ref. [15] we found that the second term in Eq. (13), $P = A_1/\lambda$, is the large-period ($P \gg 1$) approximation to the LSA's natural period. However, if $\tau_\gamma = 0$, the feedback term in the DDEs Eq. (1) becomes a modification to the linear dissipation in the LSA ODEs. Rederiving the map in Ref. [15] with this additional dissipation will recover the log term shown above. Thus, nonzero delay time affects the map through the terms with τ_γ.

IV. ANALYTICAL PREDICTIONS

The analytical approximations derived in the preceding section can be used to determine the period as a function of the pump, $P(A_1)$. We will compare the analytical results from the map (shown as thin lines in the figures) to the results of numerically simulating the original DDEs (shown as thick lines). We will first present results for long delays of $\tau = 50$ and 100, where period locking occurs (described in Sec. II), followed by short delays that do not exhibit locking. Finally, the intermediate regime that exhibits characteristics of both will be discussed.

A. Long delay: locked period

We begin with the case of $\tau = 50$ in Fig. 3(a). The thick, smoothly decreasing curve is the natural period of the LSA without DF; the nearby thin curve is from the map for $\eta = 0$ and fits the numerical result very well.

As the pump is increased from the initial locked state of $P \approx \tau$, the period approaches that of the LSA's natural period. Before exceeding the natural period, the laser's period jumps down and locks $P \approx \tau/2$. The left-most thin curve is the analytical approximation of the period from UA. For values of the pump close to threshold, $A_1 \to A_{1th}$, $\lambda \to 0$, and UA is dominated by the A_1/λ term. As the pump is increased, the period quickly asymptotes to the locked state $P \approx \tau$ ($m = 0$). For higher pump values the $m = 0$ curve intersects with the curve for the LSA's natural period. Equation () provided a condition for the maximum period, which states that the LSA's natural period is an upper bound. Thus, for higher pump values we use the lowest thin curve for the period, determined by the locking approximation LA, where $P \approx \tau/2$ ($m = 1$).

Figure 4 shows the case of $\tau = 100$, where the period locks to $P \approx 100$, 50, 33, and 25 for $m = 0$, 1, 2, and 3. We again see an excellent fit between numerical results and the map's prediction for the period. The step, or switch between analytical curves, is determined by the intersection of the locking curve with the curve for LSA's natural period.

The map does an excellent job of predicting the lock states and provides a condition for when the situation there is a step down, i.e., the LSA's natural period is an upper bound. However, the present analysis cannot predict the step up from a lower period to a higher period.

As has been demonstrated, the period of the laser in the presence of DF is determined by delay time τ. The strength of feedback η modifies period P through the small $O(\gamma)$ correction terms that we analyze in Fig. 5. We have plotted period P as a function of feedback strength η for two differ-
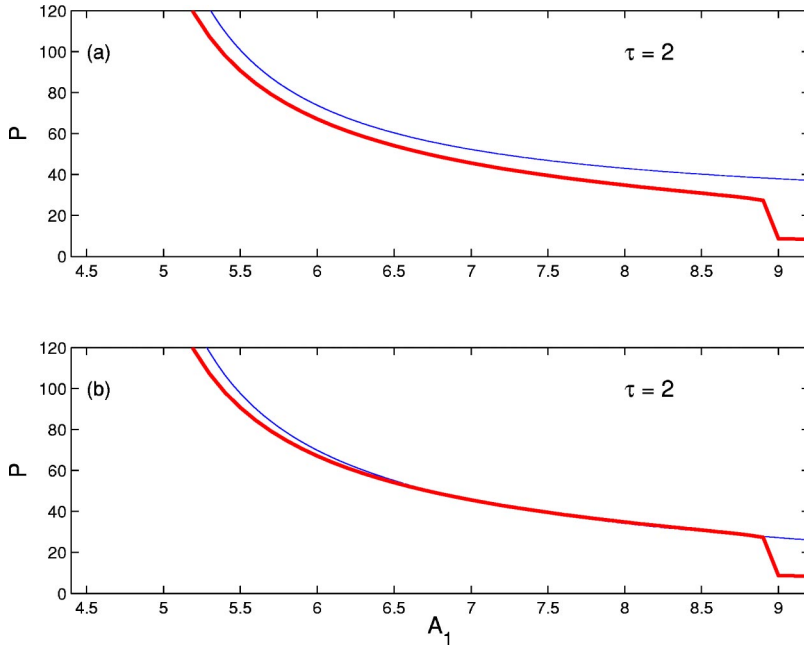
FIG. 6. For short delay, the period is shifted from the $\eta=0$ curve. The period does not become small enough before the upper Hopf bifurcation locks to an integer fraction of the delay. Thin curves, analytical; thick curves, numerical.

ent values of the pump. In Fig. 5(a), we compare numerical results (thick) to the analytical result (thin) of LA (period locking), while in Fig. 5(b), we compare to UA (decaying period). The dotted curves are shifted versions of the analytical result so that the slopes of the numerical and analytical results can be visually compared. In both cases there is a very good fit, except when feedback strength η is small. The analytical results determine that $dP/d\eta \sim 1/(\eta\lambda)$ and predict that η versus P curve decreases for increasing η. However, limit $\eta\to 0$ is singular and would require a more precise analysis to achieve a better fit in this regime.

B. Short delay: unlocked period

Figure 6 shows the case of short delay, $\tau=2$, where the LSA's natural period is always greater than the delay time, and hence, no locking will occur. (The LSA's natural period is not shown in this figure.) The analytical result UA is shown in Fig. 6(a). UA was derived with approximation $P \gg 1$ and for large period UA follows the result of numerical simulation quite well. However, it loses some fidelity for small period (large pump). This error is due to the large-period approximation used to derive UA rather than an intrinsic difficulty of the map. In Fig. 6(b) we show the result of numerically solving the implicit equation for the period, Eq. (10), before the large-period approximation is made. Here, the map result follows the numerical result extremely well, even for large pump.

C. Moderate delay

For long delays we see that the period locks to a fraction of the delay time, while for short delays the period is a perturbation of the LSA's natural period approximated by $P =A_1/\lambda$. Moderate delays exhibit both of these characteristics. Figure 7 is the case of $\tau=20$. For pump values not far from threshold, the period decays. Then, near $A_1\approx 5.9$, the period drops to the vicinity of $P\approx\tau$. As the pump increases

further, the period becomes more closely locked. The drop in the period is not a switch between two locked states, say $m =0$ and $m=1$. Rather, it occurs when the delay is long enough so that the trailing edge of the pulse $I(t-\tau)$ begins to overlap with the leading edge of the next pulse of $I(t)$. Our analysis is not yet refined enough to capture the phenomena.

The map result for UA captures the decaying period for low pump but asymptotes to a value that is too large. However, the LA ($m=0$) is more appropriate when the period is locked and gives a reasonable fit for larger pump. The main difference is due to terms $\exp(-\tau_\gamma)$ in LA, which are significant for low values of delay time.

D. Maximum pulse intensity

The maximum intensity of the pulses is an important design quantity that can also be determined from the map. The maximum occurs in the first subinterval when $dI/dT=0$, and so, from Eq. (A2), this requires $D=1$. The latter is substituted in Eq. (A3) to obtain a formula for the maximum pulse intensity in terms of the initial value of inversion D_n. For periodic solutions, the inversion is found from the period with Eq. (11), so that we have

$$I_{\max}=\frac{1}{\gamma}\{A_1(1-e^{-P})-1-\ln[A_1(1-e^{-P})]\}, \quad (14)$$

where we have kept only the large $O(1/\gamma)$ terms. The maximum intensity is affected by the delay through period P. In fact, the equation for the maximum period is the same whether delay is considered or not. That is, the maximum intensity depends directly on the period of the pulsations and only indirectly on the delay. Furthermore, for large period the dependence is weak because $\exp(-P)\ll 1$.

In Fig. 3(b) we compare the analytical and numerical results for the pulse amplitude when $\tau=50$. From Fig. 1 we
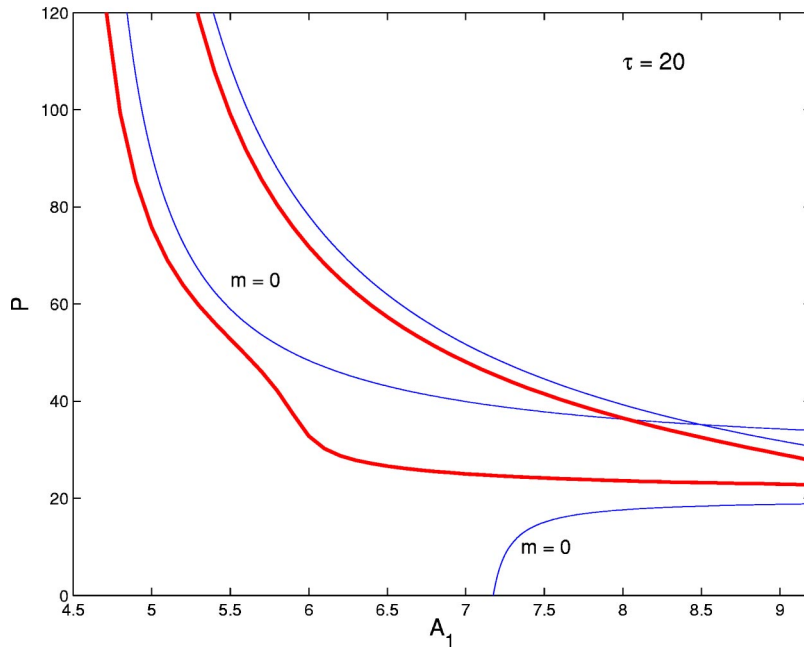
FIG. 7. For moderate delays the period first decays as the pump is increased and then abruptly drops to the $m=0$ locked state. Thin curves, analytical; thick curves, numerical.

observe that as the pump is increased, the intensity of the LSA pulses increases. Then, there is a step down in the intensity coincident with when there is a step in the period from one locked state to another. There is also a hysteresis effect when the pump is decreased.

V. DISCUSSION

Our numerical simulations illustrate locking of the LSA to the delay. We see that the LSA's natural period (no DF) serves as an upper bound for the period in the presence of delay. This causes the period to switch between different locked states as the pump is increased. There is a hysteresis effect as the pump is decreased and the laser again switches between locked states. Our analysis accurately predicts the locked states as well as the step down in period for increasing pump; however, we are not yet able to describe hysteresis. For moderate and low delay times, we can accurately described the smooth decay in the period for increasing pump.

There are two transition regions where more detailed and specialized analysis is warranted. The first is the transition between different locked regions, for example, when $m=0$ and $m=1$. Our analysis assumes that the real and delayed pulses occur in nonoverlapping time intervals. However, the transition between locked states occurs when the period is nearly a multiple of the delay so that there is overlap between the next pulse and the delayed pulse. A second type of transition occurs for intermediate delays such as case $\tau=20$. There was a jump down from an exponential decaying period to a locked period for $m=0$. Here again, this transition occurs as the delayed-pulse interval overlaps with the next pulse. Analysis of these transitions will require reexamining inner regions in the matched asymptotics construction of the map.

For self-pulsing semiconductor lasers the models can include additional terms to account for nonlinear gain satura-

tion, nonlinear damping of the active and passive regions and cross-diffusion of the carriers between active and passive regions. More importantly, the linewidth enhancement factor (LWEF) or Henry parameter α [21] is absent from our model. Including the LWEF requires that we consider the complex electric field and the evolution of the phase. Preliminary numerical simulations indicate that the locking phenomena we describe here remains valid. However, that analysis is more difficult and we postpone this consideration to a future work.

DF has been used in applications to reduce frequency jitter due to stochastic noise [22]. The period locking we describe also indicates how DF can be used to reduce the potentially deleterious effects of parameter drift due to noise. For example, the natural period of the laser is highly dependent on the pump as it varies from unbounded at threshold to an $O(1)$ value at the upper Hopf bifurcation point. With DF, the period is locked to a fixed value over a wide range of pump values. On the other hand, the hysteresis effect is the basic dynamical mechanism on which to design an optical switch. When the pump is tuned near the switch point, only small variations of the pump would be needed to switch the period of the pulsating output.

ACKNOWLEDGMENT

APPENDIX A: CONSTRUCTION OF THE MAP

In this section we describe the details of constructing the map. This involves approximating the LSA DDEs on each subinterval to account for small or large terms. The subintervals are referenced according to Fig. 2.

The pulse period is typically very large with $O(1)$ pulse widths. It is more convenient for our analysis to rescale time

so that the period is $O(1)$ while the pulse width is very small. We let $T=\gamma t$ and obtain

$$\frac{dI}{dT}=\frac{1}{\gamma}\left[\left(D+\frac{A_2}{1+aI}-1\right)I+\eta I(T-\tau_\gamma)\right],$$

$$\frac{dD}{dT}=A_1-(1+I)D, \tag{A1}$$

where $\tau_\gamma=\gamma\tau$.

$T\in[T_0,T_0']$: Define time $T=T_0$ and $T=T_0'$ as the start and end of the present pulse; in general, T_n and T_n' are the start and end of pulses $n=1,2$, etc. During the first pulse the intensity is very large, $I(T)\gg1$, and we assume the delayed pulse has not yet been reinjected into the laser and is small, $I(T-\tau_\gamma)\ll1$. The LSA equations are approximated as

$$\frac{dI}{dT}=\frac{1}{\gamma}(D-1)I, \quad \frac{dD}{dT}=ID. \tag{A2}$$

These can be solved in the phase plane by determining the equation for dI/dD, whose solution is

$$I(T)-I(T_0)=\frac{1}{\gamma}\left[-[D(T)-D(T_0)]+\ln\left(\frac{D(T)}{D(T_0)}\right)\right]. \tag{A3}$$

Time T_0' is defined as when the intensity has returned to its initial value, $I(T_0')=I(T_0)$. Thus, the inversion evolves during the pulse according to

$$0=-[D(T_0')-D(T_0)]+\ln\left(\frac{D(T_0')}{D(T_0)}\right).$$

$T\in[T_0',T_0+\tau_{\gamma'}]$. The next interval from $T=T_0'$ to $T=T_0+\tau_\gamma$ is when both the intensity and the delayed intensity are small; $I(T)\ll1$ and $I(T-\tau_\gamma)\ll1$. On this interval we solve

$$\frac{1}{I}\frac{dI}{dT}=\frac{1}{\gamma}(D+A_2-1), \quad \frac{dD}{dT}=A_1-D,$$

with initial conditions $I(T_0')=I(T_0)$ and $D(T_0')=D(T_0')$, which are determined by the terminal values of the previous interval. The equation for D can be solved first and the result used to solve for I. The solutions are

$$D(T_0+\tau_\gamma)=A_1+[D(T_0')-A_1]e^{-(T_0+\tau_\gamma-T_0')},$$

$$\gamma\ln\left(\frac{I(T_0+\tau_\gamma)}{I(T_0)}\right)=[A_1-(1-A_2)](T_0+\tau_\gamma-T_0')$$

$$-[D(T_0')-A_1](e^{-(T_0+\tau_\gamma-T_0')}-1). \tag{A4}$$

$T\in[T_0+\tau_\gamma,T_0'+\tau_\gamma]$. The effect of the delayed pulse occurs during interval $T=T_0+\tau_\gamma$ to $T=T_0'+\tau_\gamma$ when $I(T)\ll1$ but $I(T-\tau_\gamma)\gg1$. On this interval we solve

$$\frac{dI}{dT}=\frac{\eta}{\gamma}I(T-\tau_\gamma), \quad \frac{dD}{dT}=A_1-D, \tag{A5}$$

with initial conditions $I(T_0+\tau_\gamma)$ and $D(T_0+\tau_\gamma)$. Each equation can be solved independently to give

$$D(T_0'+\tau_\gamma)=A_1+[D(T_0+\tau_\gamma)-A_1]e^{-(T_0'-T_0)},$$

$$I(T_0'+\tau_\gamma)-I(T_0+\tau_\gamma)=\frac{\eta}{\gamma}\int_{T_0}^{T_0'}I(T)dT=\frac{\eta}{\gamma}p. \tag{A6}$$

The effect of the delay is to cause a jump in the intensity, proportional to the area of the original pulse. The latter can be thought of as the energy in the pulse. If there is no feedback ($\eta=0$), there is effectively no change in the intensity over the very small time interval defined by the width of the pulse.

$T\in[T_0'+\tau_\gamma,T_1]$. Finally, the last time interval is from the end of the delayed pulse, $T=T_0'+\tau_\gamma$ to the start of the next real pulse at $T=T_1$. Time T_1 is defined as when the intensity is equal to that at the start of the preceding pulse, i.e., $I(T_1)=I(T_0)$. Both the pulse and the delayed pulse are small and we solve the same equations as during $T\in[T_0',T_0+\tau_\gamma]$. We find that

$$D(T_1)=A_1+[D(T_0'+\tau_\gamma)-A_1]e^{-(T_1-T_0'-\tau_\gamma)},$$

$$\gamma\ln\left(\frac{I(T_0)}{I(T_0'+\tau_\gamma)}\right)=[A_1-(1-A_2)](T_1-T_0'-\tau_\gamma)$$

$$-(D(T_0')-A_1)[e^{-(T_1-T_0')}-e^{-\tau_\gamma}].$$

The map is determine by finding a relationship for $D(T_1)$ and T_1 in terms of $D(T_0)$ and T_0. These values of $D_n=D(T_n)$, $n=0,1,2,\dots$ correspond to the maximum of the population inversion. The minimum values of the inversion are given by $G_n=D(T_n')$, $n=0,1,2,\dots$. In constructing the map we use the fact that the width of the pulse in time scale T is $O(\gamma)$ and thus, can be ignored. Also, times T_n are defined by when the intensity reaches a fixed value, which, for algebraic convenience, we set such that $I(T_n)=I(T_0)=1$. [Analysis of the map shows that $dP/dI(T_0)=O(\gamma)$. That is, changing the value of the intensity that is used as the starting point of the pulse causes only small changes in the period.] After eliminating as many intermediate variables as possible, the map is given by

$$D_{n+1}=A_1+(G_n-A_1)e^{-P_n}, \tag{A7}$$

$$T_{n+1}=T_n+P_n, \tag{A8}$$

$$0=\ln\left(\frac{G_n}{D_n}\right)-(G_n-D_n),$$

$$\frac{\eta}{\gamma}p_n=e^{C_1}-e^{C_2},$$

$$D_n - p_n = D_n e^{-p_n}, \tag{A9}$$

$$C_1 \gamma = -\lambda(P_n - \tau_\gamma) + (G_n - A_1)(e^{-P_n} - e^{-\tau_\gamma}),$$

$$C_2 \gamma = \lambda \tau_\gamma + (G_n - A_1)(1 - e^{-\tau_\gamma}),$$

$$\lambda = A_1 - A_{1th} = A_1 - (1 - A_2). \tag{A10}$$

The effect of the delay is accounted for by variable p_n defined in Eq. (A6). However, instead of computing this integral, we follow the approach in Refs. [11–13]; use Eq. (A2) in the pulse interval $T \in [T_0, T_0']$ to determine Eq. (A9) above.

The map in Eq. (A7)–(A10) assumes that the delay pulse occurs before the next pulse, i.e., $\tau_\gamma < P_n$. These are referred to as "slowly oscillating" (SO) solutions by Grigorieva *et al.* [11–13]. For longer delays there may be two or more pulses per delay interval; these are referred to as "fast oscillating" (FO) solutions. For FO solutions, if $P_n < \tau_\gamma < P_n + P_{n-1}$ then the pulse at T_{n-1} affects the evolution from T_n to T_{n+1}. For a given τ_γ it may be the pulse starting at T_{n-m} that affects the present interval starting at T_n.

The method used to construct the map for FO solutions is the same as that for SO solutions, under the assumption that the energy in the previous pulses, $p_{n-m}, p_{n-m+1}, \ldots, p_{n-1}$, and the time intervals between them, P_{n-m}, $P_{n-(m+1)}, \ldots, P_{n-1}$, are known.

$$D_{n+1} = A_1 + (G_n - A_1)e^{-P_n},$$

$$T_{n+1} = T_n + P_n,$$

$$0 = \ln\left(\frac{G_n}{D_n}\right) - (G_n - D_n),$$

$$\frac{\eta}{\gamma} p_{n-m} = e^{C_1} - e^{C_2},$$

$$D_n - p_n = D_n e^{-p_n},$$

$$C_1 \gamma = -\lambda(P_n - \xi_n) + (G_n - A_1)(e^{-P_n} - e^{-\xi_n}),$$

$$C_2 \gamma = \lambda \xi_n + (G_n - A_1)(1 - e^{-\xi_n}),$$

$$\xi_n = \begin{cases} \tau_\gamma - \sum_{j=1}^{m} P_{n-j}, & m \geq 1 \\ \tau_\gamma, & m = 0. \end{cases}$$

The map determines the next value of inversion D_{n+1} and time T_{n+1} in terms of previous values, as defined by Eqs. (2) and (3). The delay is accounted for by variable p_{n-1}, corre-

sponding to the energy of the pulse at T_{n-m}. Likewise, τ_γ has been replaced by ξ_n defined by Eq. (4). The FO map reduces to the SO map when $m = 0$. Hence, our attention will focus on Eqs. (2)–(4) for further analysis.

Last, the asymptotic validity of the map provides a condition on the period. Interval $T \in [T_0', T_0 + \tau_{\gamma'}]$ is the time after the end of the pulse and before the delayed pulse becomes large. Both $I(T)$ and $I(T - \tau_\gamma)$ are small ($\ll 1$) on this interval. However, the pulse grows exponentially on this interval, according to Eq. (A4). At first, the net increase is very small. However, it will eventually become large enough to initiate the next pulse at T_1. For the map construction to remain valid, we require that the delayed pulse occurs before the intensity starts to grow. This will be true if the right-hand side of Eq. (A4) remains negative on the interval. To analyze this condition, we assume periodic solutions and let $G \approx 0$ (the minimum of the inversion). We obtain

$$\lambda(\tau_\gamma - mP) - A_1(1 - e^{-(\tau_\gamma - mP)}) < 0. \tag{A11}$$

For locked solutions $m \geq 1$, $(m+1)P - \tau \approx 0$, and for unlocked solutions $m = 0$ with large pump, $\tau_\gamma \approx P$. In each case the condition reduces to

$$\lambda P - A_1(1 - e^{-P}) < 0,$$

which is identical to Eq. (9).

APPENDIX B: APPROXIMATIONS

Periodic solutions of the laser correspond to fixed points of the map that are described by conditions (5) and the auxiliary equations that follow. Three approximations are used to simplify the conditions to obtain a single implicit equation for the period P given by Eq. (10).

The first approximation is to assume that the period is bound away from and below the $\eta = 0$ curve. Specifically, assume that the exp[ ] term on the right-hand side is small. Then the equation for the period reduces to $C_1(P) = \ln[(\eta/\gamma)p]$. This equation is undefined for $\eta = 0$ and we expect that subsequent results will be singular in this limit. Proper examination the case of $\eta p/\gamma \to 0$ requires that the contribution of $[1 - \exp(C_2 - C_1)]$ be included.

The second approximation applies to Eq. (6) for G, the minimum of the population inversion. For pulsating solutions the minimum is very close to zero. Thus, $G \ll |\ln G|$ in Eq. (6) leads to approximation $G \approx De^{-D}$, which fits Eq. (6) for even moderate values of D. For physically realistic values of D, say, $D > 3.5$, we can take $G \approx 0$.

Finally, we assume that the energy in the pulses is large enough so that $\exp(-p) \ll 1$. Then, $p \approx D$. Again, this approximate result fits Eq. (8) well for reasonable values of D.

[1] A. E. Siegman, *Lasers* (University Science Books, 1986).

[2] P. Mandel. *Theoretical Problems in Cavity Nonlinear Optics* (Cambridge University Press, New York, 1997).

[3] F.T. Arecchi, G.L. Lippi, G.P. Poccioni, and J.R. Tredicce, Opt. Commun. **51**, 308 (1984).

[4] K. Ikeda, Opt. Commun. **30**, 257 (1979).

[5] S. Hammel, C.K.R.T. Jones, and J. Moloney, J. Opt. Soc. Am. B **2**, 552 (1985).

[6] E. Ott, *Chaos in Dynamical Systems* (Cambridge University Press, Cambridge, 1993).

[7] F.T. Arecchi, G. Giacomelli, A. Lapucci, and R. Meucci, Phys. Rev. A **43**, 4997 (1991).

[8] R. Lang and K. Kobayashi, IEEE J. Quantum Electron. **16**, 347 (1980).

[9] G.H.M. van Tartwijk and M.S. Miguel, IEEE J. Quantum Electron. **32**, 1191 (1996).

[10] T.W. Carr, Eur. Phys. J. D **19**, 245 (2002).

[11] E.V. Grigorieva, S.A. Kahchenko, N.A. Loiko, and A.M. Samson, Physica D **59**, 297 (1992).

[12] E.V. Grigorieva and S.A. Kashchenko, Int. J. Bifurcation Chaos Appl. Sci. Eng. **3**, 1515 (1993).

[13] E.V. Grigorieva, Opt. Commun. **102**, 182 (1993).

[14] D. Pieroux and T. Erneux, Phys. Rev. A **53**, 2765 (1996).

[15] T.W. Carr and T. Erneux, Eur. Phys. J. D **17**, 67 (2001).

[16] T.W. Carr and T. Erneux, IEEE J. Quantum Electron. **37**, 1171 (2001).

[17] T. Erneux, J. Opt. Soc. Am. B **5**, 1063 (1988).

[18] L.F. Shampine and S. Thompson, Appl. Numer. Math. **37**, 441 (2001); see also http://www.cs.runet.edu/thompson/webddes/index.html

[19] J. Kevorkian and J. D. Cole, *Multiple Scale and Singular Perturbation Methods* (Springer-Verlag, New York, 1996).

[20] T.W. Carr, L. Billings, I.B. Schwartz, and I. Triandaf, Physica D **147**, 59 (2000).

[21] C.H. Henry, IEEE J. Quantum Electron. **18**, (1982).

[22] G. P. Agrawal and N. K. Dutta, *Long-Wavelength Semiconductor Lasers* (Reinhold, New York, 1986).

[23] E. J. Doedel, A. R. Champneys, T. F. Fairgrieve, Y. A. Kuznetsov, B. Sandstede, and X. Wang, AUTO97; see http://indy.cs.concordia.ca/auto